Solvent Effect on Intramolecular Long-Range Electron-Transfer Reactions between Porphyrin and Benzoquinone in an Acetonitrile Solution: Molecular Dynamics Calculations of Reaction Rate Constants

Shigehiko Hayashi[†] **and Shigeki Kato***

Department of Chemistry, Graduate School of Science, Kyoto University, Kitashirakawa, Sakyo-ku, Kyoto 606, Japan

Received: January 28, 1998

The reaction mechanism of long-range intramolecular electron transfer between the porphyrin−benzoquinone donor−acceptor pair linked by an organic spacer in acetonitrile solvent is investigated theoretically. The rate formula is derived on the basis of Fermi's golden rule for reactions induced by the through space and through bond type electronic couplings involving the dynamical effects of solvent fluctuation. Molecular dynamics (MD) calculations are carried out to construct the reaction free energy curves. The reaction rate is estimated on the basis of the results of MD calculations. It is found that there are important contributions from the vibrationally induced couplings by the solvent fluctuation. In order to examine the solvent fluctuation effect, we determine the effective electronic coupling element (ECE) and perform the decomposition analyses. The important electron pathway in determining the solvent-induced ECE is discussed.

1. Introduction

Long-range intramolecular electron-transfer process between electron donor (D) and acceptor (A) species linked by spacer (Sp) molecules has been a matter of considerable current interest.[1] As the electronic coupling between the reactant (R) and product (P) states is weak owing to the long distance between D and A, the reaction rate of electron transfer is given by Fermi's golden rule

$$k = \frac{2\pi}{\hbar}\langle |T_{PR}|^2 \{\mathrm{FCWD}\}\rangle_R \qquad (1)$$

where T_{PR} is the electronic coupling element (ECE) between R and P and FCWD the Franck−Condon weighted density, respectively. $\langle\rangle_R$ denotes the thermal average for the reactant state. Equation 1 implies that the reaction rate is characterized by the two factors T_{PR} and FCWD. T_{PR} is mainly attributed to the superexchange or indirect interaction involving the intermediate states (I) where the spacer orbitals are occupied by the electron being transferred. The other factor FCWD is concerned with the dynamics along reaction coordinates. In polar medium, the solvation coordinate is adopted as the reaction coordinate and the free energies of R and P states are represented by harmonic functions of the solvation coordinate. Using molecular simulation techniques such as molecular dynamics (MD) and Monte Carlo calculations, the mechanism of intramolecular electron transfer has been extensively examined for realistic systems from a microscopic point of view.[4−8] However, many studies have been carried out employing the standard formula of the transition-state theory (TST) in the high-temperature limit with the Condon approximation[2,3]

$$k \simeq \frac{2\pi}{\hbar}|T_{PR}|^2 \langle \{\mathrm{FCWD}\}\rangle_R \qquad (2)$$

and the two factors, T_{PR} and FCWD, have been discussed separately.

In the present study, we performed MD calculations for the photoinduced electron transfer of the porphyrin−quinone system in acetonitrile solvent. This has received much attention as a model of photosynthetic systems.[9] We develop a reaction model with the MD calculations based on a realistic molecular model constructed with the aid of ab initio molecular orbital (MO) calculations in the previous paper.[10] We focus here on the effect of solvent dynamics on the ECE, which is not taken account of within the Condon approximation. Since the charge distributions of the R, P, and I states are much different from one another in the present system, the solute−solvent interaction energies are considered to be strongly dependent on the solute electronic states. It is therefore expected that the indirect ECE is affected by the solvent fluctuation,[2,11,12] because the magnitude of indirect ECE depends on the energy differences between those states. In order to understand the reaction mechanism involving the effect of solvent fluctuation, we calculate the reaction rate beyond the Condon approximation by accommodating the scheme proposed by Freed et al.[13] for nonradiative transition processes in the gas phase.

The effect of solvent on the ECE has been discussed by Marcus and Sutin[2] and Kuzuetsov and Ulstrap[11] by considering the stabilization of reactant, product, and intermediate energy levels appearing in the McConnell-type ECE.[14] Although these studies have revealed the significance of solvation, it seems to be difficult to apply these treatments directly to realistic molecular systems. The present study is aimed to give a microscopic description of the reaction process in a realistic system based on the well-defined electronic wave functions.

In the following section, we provide a brief description of the molecular model. In section 3, we derive the rate expression including the solvent fluctuation effect on the ECE. The results of MD simulation calculations are presented in section 4. Section 5 contains the calculations of reaction rate and the analyses of the reaction mechanism. Concluding remarks are summarized in section 6.

[†] Research Fellow of the Japan Society for the Promotion of Science.

S1089-5639(98)00934-7 CCC: $15.00 © 1998 American Chemical Society
Published on Web 04/15/1998

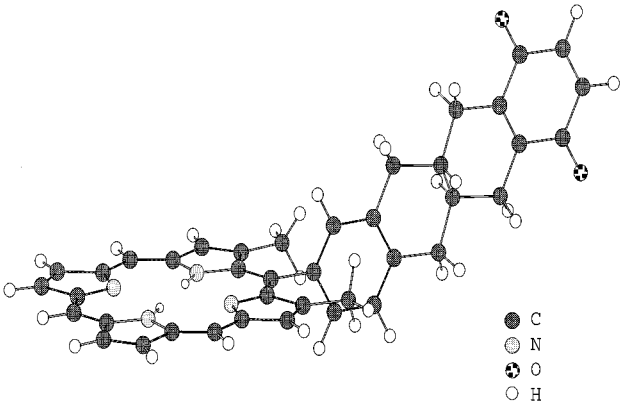

Figure 1. Geometry of the solute molecule.

2. Molecular System

We consider the porphyrin−quinone compound linked by the spacer solvated in acetonitrile solvent. The spacer consists of benzene and decalin rings as shown in Figure 1. The geometry of solute is determined by the ab initio MO calculations reported in ref 10. The electronic Hamiltonian for the solute is given by

$$\hat{H}_{\text{solute}} = \hat{W}^0 + \hat{V} \tag{3a}$$

$$\hat{W}^0 = \sum_I |\phi_I\rangle W_I^0 \langle\phi_I| \tag{3b}$$

$$\hat{V} = \sum_{I,J} |\phi_I\rangle V_{IJ} \langle\phi_J| \tag{3c}$$

where $\hat{W}^0$ represents the diagonal elements of Hamiltonian matrix defined in terms of the solute diabatic electronic states. W_I^0 is the energy of the diabatic state I in the gas phase. The off-diagonal element between the diabatic state I and J. V_{IJ}, represents the electronic coupling responsible for the intramolecular electron transfer.

In describing the electronic structures of diabatic states, we employed singly excited configuration interaction (SECI) wave functions. The reactant and product electronic states were described by the singly excited configurations from the π orbitals to the π^* ones in the porphyrin part and to the π^* ones in the quinone part, respectively. We defined 50 intermediate states that correspond to the single electron excitations from the π orbitals of porphyrin to the remaining unoccupied orbitals including the skeleton σ^* and benzene π^* orbitals in the spacer.

We employed the localized orbitals in constructing the SECI wave functions.[15] These were determined using Boys localization procedure. For the antibonding orbitals, the valence space was defined with the use of the natural localized antibonding orbitals. It can be shown that the diabatic state functions are stable to the electrostatic field coming from polar solvent.

Unfortunately, the SECI calculations provide only qualitative electronic energy levels as is well-known. We therefore adjusted the energy difference between the reactant and product states in the gas phase, ΔW^0, using the experimental values

$$\begin{aligned}\Delta W^0 &\equiv W_p{}^0 - W_R{}^0 \\ &= \text{IP(D)} - \text{EA(A)} + E_{\text{DA}}^{\text{Coulomb}} - \text{EE(D)}\end{aligned} \tag{4}$$

where IP(D) is the ionization potential of tetraethylporphyrin, 6.20 eV,[16] EA(A) the electron affinity of benzoquinone, 1.91 eV,[17] and EE(D) the first excitation energy of porphyrin, 2.01 eV,[18] respectively. $E_{\text{DA}}^{\text{Coulomb}}$ represents the electrostatic interaction between D and A in the product state, which was approximated by the Coulomb interaction energy between the unit point charges located on the centers of the porphyrin and benzoquinone moieties in the total system. As the result, $E_{\text{DA}}^{\text{Coulomb}}$ was estimated to be −1.10 eV, and the resultant ΔW^0 became 1.18 eV. The gas-phase energies of the intermediate states were determined so as to reproduce the energy differences between these states and the product state obtained by the SECI calculations. The energy differences between the reactant and intermediate states are in the range of 2.94−20.5 eV.

We determined 1326 off-diagonal coupling elements V_{IJ} using the SECI wave functions. The magnitudes of these elements lie in the range of 0.00−2.99 eV.

3. Theory

3.1. Rate Expression. The reaction rate is given by Fermi's golden rule

$$k = \frac{1}{\hbar^2}\frac{1}{Z}\int_{\infty}^{-\infty} \mathrm{d}t\ \mathrm{Tr}\left[\exp\left\{-\frac{i}{\hbar}\hat{H}_R\tau\right\}T_{RP}\exp\left\{\frac{i}{\hbar}\hat{H}_P t\right\}T_{RP}\right] \tag{5}$$

where $\tau = i\hbar\beta$ and $\beta^{-1} = k_{\text{B}}T$. T is the temperature with k_{B} the Boltzmann constant. $\hat{H}_R$ and $\hat{H}_P$ are the Hamiltonians of the reactant and product states, respectively. T_{PR} is the transition matrix element, and Z is the partitioning function of the reactant state. Using the harmonic bath model to describe the fluctuation of solvent, the Hamiltonian is expressed as[19]

$$\hat{H} = \hat{K} + \hat{V} + \hat{W} \tag{6a}$$

$$\hat{K} = \int_{+0}^{\omega_{\text{cut}}} \mathrm{d}\omega\ \frac{1}{2}p^2(\omega) \tag{6b}$$

$$\hat{V} = \sum_{I\neq J} |\phi_I\rangle V_{IJ} \langle\phi_J| \tag{6c}$$

$$\hat{W} = \sum_I |\phi_I\rangle W_I(x) \langle\phi_I| \tag{6d}$$

$\hat{K}$ is the operator of the kinetic energy of bath modes. $p(\omega)$ is the conjugate momentum to the bath coordinate $x(\omega)$ whose frequency is ω. ω_{cut} is the cutoff frequency of the bath modes. $\hat{V}$ represents the operator of the electronic coupling between the diabatic states. Because the diabatic states are stable to the electrostatic field from polar solvent as mentioned in the preceding section, the dependence of V_{IJ} on the bath variables was neglected in eq 6c. The potential energy of the diabatic state I, $W_I(x)$, is expressed as

$$W_I(x) = \int_{+0}^{\omega_{\text{cut}}} \mathrm{d}\omega \left\{\frac{1}{2}\omega^2(x(\omega) - \Delta_I(\omega))^2\right\} + G_I^0 \tag{7a}$$

$$G_I^0 = W_I^0 - \int_{+0}^{\omega_{\text{cut}}} \mathrm{d}\omega\ \frac{1}{2}\omega^2\Delta_1^2(\omega) \tag{7b}$$

where W_I^0 is the gas-phase energy. Note that the bath modes are linearly coupled to the electronic states with the coupling coefficients $\Delta_I(\omega)$.

The transition matrix in solution was defined with the Hamiltonian, eq 6a. Choosing the bath coordinate x as the adiabatic parameter, the transition matrix $T_{PR}(x)$ is given by[20]

$$T_{PR}(x) = \langle\phi_P|\hat{V}|\psi_R(x)\rangle \tag{8}$$

where $|\psi_R(x)\rangle$ is the eigenfunction of Hamiltonian eq 6a for the reactant state. Since the energy differences between the reactant and intermediate diabatic states are much larger than the off-diagonal electronic coupling terms in the present case, $T_{PR}(x)$ is expressed approximately by several lower order terms in a series of the perturbation expansion where $W_R(x = \Delta_R)$ is adopted as the zeroth order Hamiltonian:[21]

$$T_{PR}(x) = T_{PR}^{(1)} + \int_{+0}^{\omega_{\rm cut}} d\omega \left\{ T_{PR}^{(2)}(\omega)(x(\omega) - \Delta_R(\omega)) + T_{PR}^{(3)} \frac{\delta}{\delta x(\omega)} + T_{PR}^{(4)} \frac{\delta^2}{\delta x^2(\omega)} \right\} \quad (9a)$$

$$T_{PR}^{(1)} = V_{PR} + \sum_{I,J\in eI} V_{PI} G_{IJ}^0 V_{JR} \quad (9b)$$

$$T_{PR}^{(2)}(\omega) = -\sum_{I,J,K\in I} V_{PI} G_{IJ}^0 \omega^2 (\Delta_J(\omega) - \Delta_R(\omega)) G_{JK}^0 V_{KR} \quad (9c)$$

$$T_{PR}^{(3)}(\omega) = \frac{\hbar^2}{2} \sum_{I,J,K,L\in I} V_{PI} G_{IJ}^0 G_{JK}^0 \omega^2 (\Delta_K(\omega) - \Delta_R(\omega)) G_{KL}^0 V_{LR} \quad (9d)$$

$$T_{PR}^{(4)} = \frac{\hbar^2}{2} \sum_{I,J,K,L\in I} V_{PI} G_{IJ}^0 G_{JK}^0 V_{KR} \quad (9e)$$

$$\hat{G}^0 = \frac{1}{\sum_{I\in I} |\phi_I\rangle [G_R^0 - W_I(x = \Delta_R)] \langle \phi_I| - \hat{V}^I} \quad (9f)$$

$T_{PR}(x)$ given by eq 9a consists of four terries. The first term, $T_{PR}^{(1)}$, is the zeroth-order term which is independent of the bath variables. The second and third terms correspond to the so-called Herzberg−Teller vibronic and non-Born−Oppenheimer couplings, respectively.[22] $\hat{G}^0$ given by eq 9f is the electronic Green function, and $\hat{V}^I$ represents the electronic coupling between the intermediate states.

Using the Hamiltonian and transition matrix given by eqs 6a and 9a, eq 5 is rewritten as[13]

$$k = \frac{1}{\hbar^2} \frac{1}{Z} \int_{-\infty}^{\infty} dt \exp\left[\frac{i\Delta G^0 t}{\hbar}\right] \lim_{N\to\infty} \int_{-\infty}^{\infty} dx_a(\omega_1) \cdots \times \int_{-\infty}^{\infty} dx_a(\omega_N) \int_{-\infty}^{\infty} dx_b(\omega_1) \cdots \times \int_{-\infty}^{\infty} dx_b(\omega_N) [T_{PR}(x_a) \rho_{\rm R}(x_a, \tau; x_b, 0)] \times [T_{PR}(x_b) \rho_{\rm p}(x_a, \tau; x_b, -t; x_a, 0)] \quad (10)$$

where ΔG^0 is the reaction free energy change, $\Delta G^0 = G_P^0 - G_R^0$. $\rho_M(x_a, t; x_b, 0)$ is the Green function of the bath modes for the reactant ($M = R$) or product ($M = P$) diabatic state

$$\rho_M(x_a, t; x_b, 0) = \prod_i^N \left(\frac{\Delta\omega\omega_i}{2\pi i\hbar \sin \omega_i t}\right)^{1/2} \times \exp\left[\frac{i\Delta\omega\omega_i}{4\hbar} \{(x_a(\omega_i) - x_b(\omega_i))^2 \cot {}^1\!/_2 \omega_i t - (x_a(\omega_i) - x_b(\omega_i) - 2\Delta_M(\omega_i))^2 \tan {}^1\!/_2 \omega_i t\}\right] \quad (11)$$

where $\Delta\omega = \omega_{\rm cut}/N$. It is noted that the Green function for each state M is characterized by the solute-solvent coupling coefficients $\Delta_M(\omega_i)$. Because T_{PR} consists of the 4 terms in eq 9a, the rate constant is expressed as the sum of 10 terms

$$k = \sum_{\substack{\alpha\beta=1 \\ \alpha\le\beta}}^{4} k_{\alpha\beta} \quad (12)$$

where $k_{\alpha\beta}$ is the term including $T_{PR}^{(\alpha)}$ and $T_{PR}^{(\beta)}$.

The analytical expression of each term in eq 12 was obtained by carrying out the integrations appearing in eq 10. It is possible to complete the integrations over x_a and x_b analytically because $\rho_M(x_a, t; x_b, 0)$ is a Gaussian function of these variables. The integration over t was accomplished by short-time approximation,[23] which gives the semiclassical expression of the reaction rate. For example, $k_{11\rm sc}$, the semiclassical form of k_{11}, is given by

$$k_{1\rm lsc} = \frac{1}{\hbar} T_{PR}^{(1)} T_{PR}^{(1)} \left(\frac{\pi}{\int_{+0}^{\omega_{\rm cut}} d\omega\, \lambda(\omega)\, k_{\rm B} T'(\omega)}\right)^{1/2} \times \exp\left[-\frac{(\Delta G^0 + \lambda)^2}{4 \int_{+0}^{\omega_{\rm cut}} d\omega\, \lambda(\omega)\, k_{\rm B} T'(\omega)}\right] \quad (13)$$

where $\lambda(\omega)$ and λ are the reorganization energies of the bath mode ω and the total bath modes, respectively

$$\lambda(\omega) = \frac{1}{2} \omega^2 \Delta_{PR}^2(\omega) \quad (14a)$$

$$\lambda = \int_{+0}^{\omega_{\rm cut}} d\omega\, \lambda(\omega) \quad (14b)$$

$$\Delta_{PR}(\omega) = \Delta_P(\omega) - \Delta_R(\omega) \quad (14c)$$

$k_{\rm B}T'(\omega)$ is the effective thermal energy defined by

$$k_{\rm B} T'(\omega) = \frac{1}{2} \hbar\omega \coth \frac{1}{2} \hbar\omega\beta \quad (15)$$

In the high-temperature limit, $\hbar\omega\beta \ll 1$, $k_{\rm B}T'(\omega)$ approaches to $k_{\rm B}T$ and the classical expression $k_{11\rm c}$ is obtained as

$$k_{11\rm c} = \frac{1}{\hbar} T_{PR}^{(1)} T_{PR}^{(1)} \left(\frac{\pi}{\lambda k_{\rm b} T}\right)^{1/2} \exp\left[-\frac{\Delta G^{\ddagger}}{k_{\rm B} T}\right] \quad (16)$$

where the activation energy $\Delta G^{\ddagger}$ is given by the Marcus relation[24,25]

$$\Delta G^{\ddagger} = \frac{(\Delta G^0 + \lambda)^2}{4\lambda} \quad (17)$$

The integration over ω was evaluated by a trapezoid formula with the finite step size $\Delta\omega$. Hereafter, the harmonic bath part of the Hamiltonian is expressed by the discretized form, i.e., $x_i = (\Delta\omega)^{1/2} x(\omega_i)$ and $\Delta_{Ii} = (\Delta\omega)^{1/2} \Delta_I(\omega_i)$.

The semiclassical and classical expressions of the main terms in eq 9a are presented in Appendix A.

3.2. Solvent Fluctuation. In evaluating the rate constant based on the formulae presented in section 3.1 and Appendix A, the frequency-dependent coupling coefficients $\{\Delta Ii\}$ are required. Note that the reorganization energy λ is deduced from the coupling coefficients of the reactant and product states as

seen in eq 14. The coupling coefficient can be formally expressed with the coupling strength factor, g_I, and the direction unit-vector in the harmonic bath space, $\tilde{\mathbf{c}}_I$

$$\Delta_{Ii} = g_I \omega_i^{-2} \mathbf{c}_{Ii} \tag{18}$$

In order to calculate the coupling coefficients from the properties of solvation obtained by MD simulations, we introduced the solvation coordinate defined by the potential energy difference between the reactant and product states.[26] Employing the potential energy functions given by eq 7, the solvation coordinate s is defined as

$$\begin{aligned} s &= W_R(\mathbf{x}) - W_P(\mathbf{x}) \\ &= \sum_i (\Delta_{Ri} - \Delta_{Pi}) \omega_i^2 \tilde{x}_i \end{aligned} \tag{19}$$

where $\tilde{\mathbf{x}}$ is the displacement of the bath coordinate from the minimum energy crossing point $\mathbf{x}^{\ddagger}$,[27,28] i.e.

$$\tilde{\mathbf{x}} = \mathbf{x} - \mathbf{x}^{\ddagger} \tag{20}$$

Equation 19 is rewritten with the direction vector of the solvation coordinate $\tilde{s}$, whose direction coincides with that of the steepest descent path at $x^{\ddagger}$

$$s = \mu^{-1/2} \sum_i \tilde{s}_i \tilde{x}_i \tag{21}$$

$$\mu = (g_R - g_P)^{-2} = \frac{k_B T}{\langle \dot{s}^2 \rangle} \tag{22}$$

where g_R and g_P are the coupling strength factors of the reactant and product and $\langle\rangle$ indicates the equilibrium thermal average. μ is regarded as the effective mass for the motion along the solvation coordinate. Using eqs18, 21, and 22, it can be shown that the direction vectors of coupling coefficients in the reactant and product states coincide with $\tilde{\mathbf{s}}$

$$\tilde{\mathbf{c}}_R = \tilde{\mathbf{c}}_P = \tilde{\mathbf{s}} \tag{23}$$

In the present case, the energy levels of the intermediate states are much higher than those of the reactant and product states so that the intermediate states can be treated as virtual states. Thus the fluctuation of the bath along $\tilde{\mathbf{s}}$ contributes dominantly to the vibrationally induced couplings. We therefore imposed the assumption that the direction vectors of the coupling coefficients in the intermediate states are the same as those of R and P. As the result, the coupling coefficients for R, P, and I are given by

$$\Delta_{Ii} = g_I \omega_i^{-2} \tilde{s}_i \tag{24}$$

As easily seen, the components of the direction vector $\tilde{\mathbf{s}}$ are given by the Fourier components of the velocity autocorrelation function of the solvation coordinate

$$\langle \dot{s}\dot{s}(t) \rangle = \frac{k_B T}{\mu} \sum_i \tilde{s}_i^2 \cos(\omega_i t) \tag{25}$$

The coupling strength factors g_I are related to the minimum positions of the free energy curves along s, $s_{\mathrm{min}I}$, as

$$s_{\mathrm{min}I} = -\mu^{-1/2} \Omega^{-2} g_I + W_R^0 - W_P^0 \tag{26}$$

For the reactant and product states, the coupling strength factors are derived from eq 26 with $s_{\mathrm{min}I}$ computed by the MD simulations

$$s_{\mathrm{min}I} = \langle s \rangle_I \quad (I = R, P) \tag{27}$$

where $\langle\rangle_I$ indicates the equilibrium ensemble average for the state I. In order to calculate the coupling strength factors for the intermediate states, we defined the coordinates given by the energy differences between the intermediate state I and the reactant (product) state, s_{RI} (s_{PI}). By projecting the direction vectors of s_{RI} and s_{PI} onto the direction $\tilde{\mathbf{s}}$, one can obtain the relation

$$g_I = \frac{1}{2} \mu^{1/2} (g_R^2 - g_P^2 - \mu_{RI}^{-1} + \mu_{PI}^{-1}) \tag{28}$$

where μ_{RI} and μ_{PI} are the effective masses for the coordinates s_{RI} and s_{PI}. The effective masses are estimated by the MD calculations

$$\mu_{MI} = k T_B \langle \dot{s}_{MI}^2 \rangle_M^{-1} \quad (M = R, P) \tag{29}$$

Once the coupling strength factors g_I and the direction vector $\tilde{\mathbf{s}}$ are obtained, the free energy curves along the solvation coordinate s can be constructed. Partitioning the bath coordinates in the Hamiltonian into s and the remaining coordinates whose directions are orthogonal to $\tilde{\mathbf{s}}$,[27,28] the free energy curve of the state I, $F_I(s)$, is expressed as

$$F_I(s) = {}^1/_2 \kappa (s - s_{\mathrm{min}I})^2 - G^{\mathrm{solv}}(s_{\mathrm{min}I}) + W_I^0 \tag{30}$$

κ is the force constant given by

$$\begin{aligned} \kappa &= (s_{\mathrm{min}P} - s_{\mathrm{min}R})^{-1} = {}^1/_2 \lambda^{-1} \\ &= \mu \Omega^2 \end{aligned} \tag{31}$$

where Ω is the effective frequency determined by

$$\Omega = \sqrt{(\tilde{s}^t \tilde{\omega}^{-2} \tilde{s})^{-1}} \tag{32}$$

Noted that κ of the reactant, product, and intermediate states are the same. $s_{\mathrm{min}I}$ is derived from g_I using eq 26. $G^{\mathrm{solv}}(s_{\mathrm{min}I})$ is the stabilization energy due to the solvation at $s = s_{\mathrm{min}I}$ as defined by the second term in the right-hand side of eq 7b and is rewritten as follows

$$\begin{aligned} G^{\mathrm{solv}}(s_{\mathrm{min}I}) &= \sum_i \frac{1}{2} \omega_i^2 \Delta_{Ii}^2 \\ &= {}^1/_2 \kappa (s_{\mathrm{min}I} - s_0^{\mathrm{solv}})^2 \end{aligned} \tag{33a}$$

$$s_0^{\mathrm{solv}} = -\Delta W^0 \tag{33b}$$

The relation

$$F_I(s_0^{\mathrm{solv}}) = W_I^0 \tag{34}$$

indicates that the free energy of each state at $s = s_0^{\mathrm{solv}}$ coincides with the energy in the gas phase.

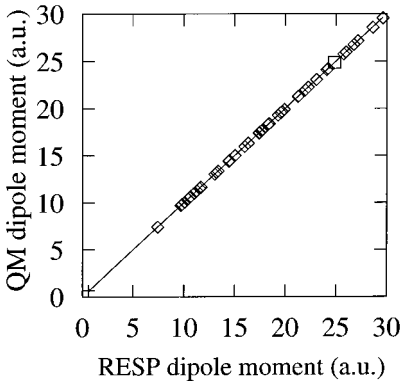

Figure 2. Comparison of dipole moments obtained by the MO calculations (QM) and the RESP method. Symbols +, □, and ◇ indicate the dipole moments of the reactant, product, and intermediate states, respectively.

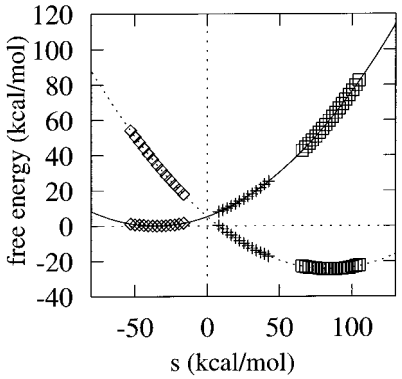

Figure 3. Free energy curves along the solvation coordinate. Solid and dashed curves are the free energies of the reactant and product states, respectively, obtained by eq 30. Symbols ◇, +, and □ indicate the free energies evaluated by eqs 36 and 37 with $\alpha = 0.0$, 0.5, and 1.0, respectively.

4. Molecular Dynamics Calculation

4.1. Potential Functions. The solute and solvent molecules were treated as rigid bodies. The solute−solvent and solvent−solvent interactions were described by pair potential functions between the interaction sites. For the solute, the interaction sites were assigned to all the constituent atoms while the three-site model was employed for acetonitrile. The pair potential is given as the sum of Coulombic and 12-6 Lennard-Jones (LJ) functions. We used the potential parameters developed by Jorgensen et al.[29] for the solvent acetonitrile. The effective charges on the interaction sites for the diabatic states of the solute molecule were determined by the restrained electrostatic potential (RESP) method.[30] In Figure 2, the dipole moments for the diabatic states evaluated with the RESP effective charges are compared with those directly obtained by the ab initio MO calculations. The dipole moments for each diabatic state are well-reproduced by the RESP effective charges. It is noteworthy that the dipole moments distribute widely in the range of 0−30 au. We used the LJ parameters of AMBER4[31] for the solute atoms, which were the same for all the diabatic states. In constructing the solute−solvent LJ functions, we took the geometric and arithmetic means for the energy and length parameters, respectively, as usual.

Since the present molecular model involves many parameters including the electronic coupling elements and potential parameters, it is inadequate to list them in this article. These parameters are available from the authors upon request.

4.2. Computational Details. We carried out MD calculations for one solute and 2019 solvent molecules. The simulation box length was set to 56.3 Å. The long-range Coulombic interactions between solvent−solvent and solute−solvent were computed by the Ewald sum method and the reaction field with potential tapering, respectively. We employed the leap frog algorithm for the integration of the equations of motion. The equilibrium MD runs of 40 ps following after the cooling and equilibration runs of 15 ps were performed with the time step of 0.5 fs. Good energy conservation was achieved; the standard deviation from the average total energy was 4.0×10^{-3} kcal/mol. Temperature control algorithms were not applied. The average temperature was 297 K, and the standard deviation was 3 K.

4.3. Results of MD Calculation. *4.3.1. Free Energy Curves of R and P.* The free energy curves of the reactant and product states along *s* were obtained by the MD calculations for each state. If we employ the harmonic bath model in describing the fluctuation of solvent, the free energy curves are expressed by eq 30. Using the calculated values of $s_{\min R}$ and $s_{\min P}$, we constructed the reactant and product free energy curves as in Figure 3. These free energy curves were compared with those derived from the probability densities of *s*. The equilibrium MD calculations were carried out with the Hamiltonian including a window parameter α[28]

$$H^{\mathrm{MD}} = T^{\mathrm{MD}} + \alpha(W_P^{\mathrm{MD}} - W_R^{\mathrm{MD}}) + W_R^{\mathrm{MD}} \qquad (35)$$

where T^{MD} and W_M^{MD} are the kinetic energy and the potential energy of the *M* state employed in the MD calculations, respectively. The free energy curve with the parameter α is given by

$$F(s, \alpha) = -k_{\mathrm{B}}T \ln P(s, \alpha) + C(\alpha) \qquad (36)$$

where $P(s, \alpha)$ *is* the probability density of *s* and $C(\alpha)$ is a constant. Note that there is the relation between $F(s, \alpha)$ and $F(s, 0)$ as

$$F(s, \alpha) - F(s, 0) = -\alpha s \qquad (37)$$

Figure 3 also includes the free energy curves derived from $F(s, \alpha)$ with the relation of eq 37 for $\alpha = 0$, $^1/_2$, and 1. As is easily seen, both free energies, $F_M(s)$ and $F(s, \alpha)$, are in good agreement with each other, indicating the validity of the assumption of linear response to describe the fluctuation of solvent.

The reorganization energy λ and exothermicity $-\Delta G^0$ were calculated to be 60.2 and 24.5 kcal/mol, respectively. It is noteworthy that the reaction is endothermic in the gas phase as shown by eq 4, and the solvation makes the reaction exothermic. The activation barrier height $\Delta G^{\ddagger}$ of 5.3 kcal/mol was estimated by eq 17.

4.3.2. Coupling Coefficient. As shown in eq 24, the coupling coefficients Δ_I consist of the direction vector $\tilde{\mathbf{s}}$ and the coupling strength factor g_I. The components of solvation coordinate, $\tilde{s}_i^2$, were computed by the relation of eq 25 with the velocity autocorrelation functions of *s*. In Figure 4, the components derived from the MD simulations for the reactant and product states are displayed. The distributions of components for *R* and *P* are similar to each other. It is roughly characterized by a peak centered at about 100 cm^{-1}, which is consistent with the experimental findings of the far-infrared absorption spectrum.[32]

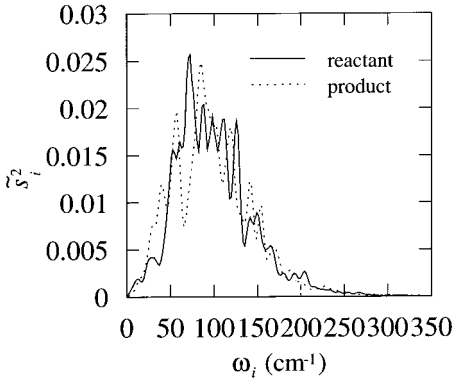

Figure 4. Components of the direction vector $\tilde{\mathbf{s}}$ computed by eq 25 with the velocity correlation functions of s obtained by the MD calculations for the reactant (solid line) and product (dashed line) states.

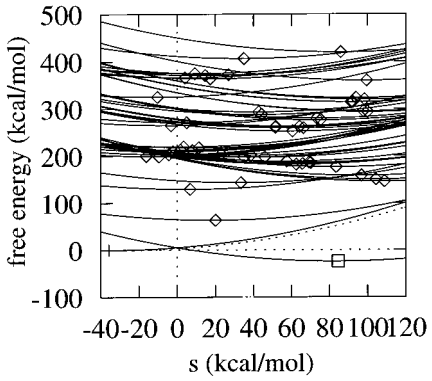

Figure 5. Free energy curves $F_I(s)$ defined by eq 30 (solid lines) and stabilization energy $G^{\mathrm{solv}}(s)$ by eq 33a (dashed line). Symbols ×, □, and ◇ indicate the minimum free energies, $F_I(s_{\mathrm{min}I})$, for the reactant, product, and intermediate states, respectively. The force constant κ and minimum positions $s_{\mathrm{min}I}$ are evaluated with the direction vector $\tilde{\mathbf{s}}$ and coupling strength factors g_I (see section 4.3).

TABLE 1: Effective Frequency (cm^{-1})

	R	P
Ω	49.8	56.2
Ω	57.6	58.4

We calculated the effective frequency Ω by two different relations, eq 32 and

$$\Omega' = \sqrt{\langle \dot{s}^2 \rangle / \langle \delta s^2 \rangle} \tag{38}$$

The resultant frequencies for R and P are summarized in Table 1, where it is found that the frequencies for R and P are very close to each other and are almost independent of the definitions, eqs 32 and 38. These results imply that the harmonic bath model is a good approximation to describe the fluctuation of the solvation coordinate.

The coupling strength factors for the reactant and product states, g_R and g_P, were derived from $s_{\mathrm{min}R}$ and $s_{\mathrm{min}P}$ using eq 26. For the intermediate states, on the other hand, the coupling strength factors, g_I, were first computed with the use of eqs 28 and 29 and were used to estimate $s_{\mathrm{min}I}$ with eq 26.

Figure 5 shows the free energy curves of reactant, product, and intermediate states, $F_I(s)$, obtained by eq 30. As mentioned in section 3.2, the free energy curves for all the states have the same force constant κ. s_0^{solv} was evaluated to be −27 kcal/mol. The calculated values of $s_{\mathrm{min}I}$ distribute widely in the range of $s = -40-110$ kcal/mol. We found three low lying intermediate states in which the π^* orbitals in the benzene part are occupied.

TABLE 2: Reaction Rate (s^{-1})

	$k_{\alpha\beta}$	$\lvert k_{\alpha\beta}/k \rvert$		$k_{\alpha\beta}$	$\lvert k_{\alpha\beta}/k \rvert$
k_{sc}	5.37×10^5		$k_{13\mathrm{sc}}$	-2.70×10^1	<0.001
k_{c}	5.16×10^5		$k_{13\mathrm{c}}$	-2.63×10^1	<0.001
$k_{\mathrm{sc}}/k_{\mathrm{c}}$	1.05		$k_{13\mathrm{sc}}/k_{13\mathrm{c}}$	1.03	
$k_{11\mathrm{sc}}$	3.40×10^5	0.633	$k_{14\mathrm{sc}}$	3.07×10^2	0.001
$k_{11\mathrm{c}}$	3.27×10^5	0.634	$k_{14\mathrm{c}}$	3.01×10^2	0.001
$k_{11\mathrm{sc}}/k_{11\mathrm{c}}$	1.04		$k_{14\mathrm{sc}}/k_{14\mathrm{c}}$	1.02	
$k_{12\mathrm{sc}}$	1.75×10^5	0.326	$k_{22\mathrm{sc}}$	2.13×10^4	0.040
$k_{12\mathrm{c}}$	1.68×10^5	0.325	$k_{22\mathrm{c}}$	2.04×10^4	0.040
$k_{12\mathrm{sc}}/k_{12\mathrm{c}}$	1.04		$k_{22\mathrm{sc}}/k_{22\mathrm{c}}$	1.04	

These benzene π^* orbitals were diabatized by diagonalizing the dipole operator along the C_2 axis of the partial system defined by excluding the dimethylporphyrin part from the total system.[10] One of these intermediate states is described by the electron excitation to the π^* orbital having b symmetry ($F_I(s_{\mathrm{min}I}) \sim 50$ kcal/mol) and the other two are by the excitation to the a symmetry π^* orbitals ($F_I(s_{\mathrm{min}I}) \sim 130$ kcal/mol), respectively. Although the former has lower energy, the electronic coupling with the product states is small because the π^* orbital of the benzoquinone included in the product state has a symmetry. The intermediate states with $F_I(s_{\mathrm{min}I})$ in the range of 150−200 kcal/mol include the C−H σ^* antibonding orbitals. Those with $F_I(s_{\mathrm{min}I}) = 250-300$ kcal/mol correspond to the excitations to the C−C σ^* orbitals except for the benzene and benzoquinone skeleton σ^* orbitals. These skeleton C−C σ^* orbitals are involved in the states with $F_I(s_{\mathrm{min}I}) > 300$ kcal/mol.

5. Reaction Rate

The reaction rate of intramolecular electron transfer was evaluated using the electronic coupling elements between the diabatic states represented by $\hat{V}$ and $\hat{G}$ and the coupling coefficients between the electronic states and the bath coordinates, Δ_I (see eqs 12−17 and Appendix A). We used the results of MO and MD calculations for these quantities as presented in sections 2 and 4.3.2, respectively. The temperature was set to be $T = 297$ K. The cutoff value of frequency, ω_{cut}, was chosen to be 400 cm^{-1} and that of the number of solvent bath modes to be 200, respectively. Although the solvation coordinate vector $\tilde{\mathbf{s}}$ is slightly different for the reactant and product states as shown in Figure 4, both the vectors gave essentially the same rate constant. Therefore we only present the results with the use of reactant-state solvation coordinate vector.

As is shown in eq 9a, $T_{PR}^{(1)}$ is regarded as the zeroth-order term of the perturbation expansion of T_{PR}. At first, we estimated the lower order terms of k including $T_{PR}^{(1)}$, i.e., k_{11}, k_{12}, k_{13}, and k_{14}, with both the semiclassical and classical expressions. The resultant reaction rates are summarized in Table 2. Because k_{13} and k_{14} are much smaller than k_{11} and k_{12}, we omitted to evaluate the higher order terms including $T_{PR}^{(3)}$ and $T_{PR}^{(4)}$. The second-order term for $T_{PR}^{(2)}$, k_{22}, is also given in Table 2. The total reaction rates k_{sc} and k_{c} are defined by the sum of $k_{\alpha\beta}$ appearing in Table 2.

The calculated k_{sc} is 5.37×10^5 s^{-1}, which is about 1/100 of the experimental value observed in DMF solution.[9] The calculated activation energy $\Delta G^{\ddagger}$, 5.36 kcal/mol, seems to be higher than the experimental one by about 2 kcal/mol. One of the reasons of this discrepancy may be that we neglected the effect of electronic reorganization of solute and solvent molecules particularly in the product state, and the exothermicity of reaction is estimated to be too small. Considering many approximations introduced in constructing the molecular model, which includes a large solute molecule and a number of solvent

molecules, it would be unavoidable to cause the error of 2 kcal/mol for the activation barrier height.

It is found that the semiclassical rate constant k_{sc} is slightly larger than the classical one, k_c, only by 5% indicating that vibrational quantum effects attributed to the effective thermal energies $k_B T'(\omega)$ are not important in the present case. This comes from the result that the components of the solvation coordinate vector $\tilde{\mathbf{s}}$ mainly distribute in the lower frequency range than the thermal energy $k_B T = 206$ cm^{-1} as shown in Figure 4. For simplicity, we hereafter only discuss the classical rate constant.

As seen in Table 2, the magnitude of reaction rate k_c is mainly determined by the terms k_{11c}, k_{12c}, and k_{22c}, and the contributions of k_{13c} and k_{14c} are negligibly small in the present case. We therefore analyzed the rate constant by approximating it as

$$k_c \simeq k_{11c} + k_{12c} + k_{22c} \tag{39}$$

The characters of the other terms, k_{13c} and k_{14c}, are discussed in Appendix B.

The components of rate constant are formally written by

$$k_{\alpha\beta c} = \frac{1}{\hbar}\Lambda_{\alpha\beta}\left(\frac{\pi}{\lambda k_B T}\right)^{1/2} \exp\left[-\frac{\Delta G^{\ddagger}}{k_B T}\right] \tag{40}$$

where $\Lambda_{\alpha\beta}$ are given by

$$\Lambda_{11} = T^{(1)}_{PR} T^{(1)}_{PR} \tag{41a}$$

$$\Lambda_{12} = \sum_i \sigma_{12}(\omega_i) T^{(1)}_{PR} T^{(2)\prime}_{PRi} \tag{41b}$$

$$\Lambda_{22} = \sum_{i,j} \sigma_{22}(\omega_i, \omega_j) T^{(2)\prime}_{PRi} T^{(2)\prime}_{PRj} \tag{41c}$$

$T^{(2)\prime}_{PRi}$ is regarded as the transition matrix element corresponding to the Herzberg−Teller vibronic coupling defined by eq A3. In Figure 6, the coefficients $\sigma_{12}(\omega_i)$ and $\sigma_{22}(\omega_i, \omega_i)$ are shown as the functions of bath frequencies. As seen in Figure 6a, σ_{12} is almost independent of ω_i. We showed $\sigma_{22}(\omega_i, \omega_i)$ at the fixed values of ω_j, 0 and 200 cm^{-1}, in Figure 6b, where it is found that σ_{22} is almost constant for the frequency change.

Considering these results, the coefficients σ_{12} and σ_{22} may be represented by

$$\sigma_{12}(\omega_i) = -\frac{k_B T}{2\hbar} h^{(1)} \tag{42a}$$

$$\sigma_{22}(\omega_i, \omega_j) = 2\left(\frac{k_B T}{\hbar}\right)^2 h^{(2)} \tag{42b}$$

where $h^{(1)}$ and $h^{(1)}$ are the expansion coefficients of $E(\omega)$ defined by eq A6 with respect to ω

$$E(\omega) \simeq E(0)(1 + h^{(1)}\omega + h^{(2)}\omega^2) \tag{43a}$$

$$h^{(1)} = -\frac{(\Delta G^0 + \lambda)\hbar}{2\lambda k_B T} \tag{43b}$$

$$h^{(2)} = \frac{1}{2}\left\{-\frac{\hbar^2}{2\lambda k_B T} + \left[\frac{(\Delta G^0 + \lambda)\hbar}{2\lambda k_B T}\right]^2\right\} \tag{43c}$$

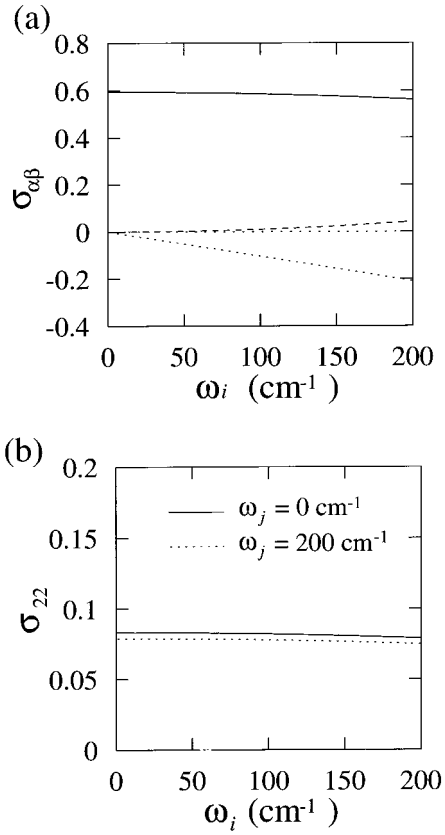

Figure 6. Coefficients $\sigma_{\alpha\beta}$. (a) Solid, dotted, and dashed lines indicate $\sigma_{12}(\omega_i)$, $\sigma_{13}(\omega_i)$, and $\sigma_{14}(\omega_i)$, respectively. (b) $\sigma_{22}(\omega_i, \omega_j)$ at $\omega_j = 0$ and 200 cm^{-1}.

Λ_{12} and Λ_{22} are thus represented by

$$\Lambda_{12} = \sum_i T^{(1)}_{PR} \tilde{T}^{(2)}_{PRi} \tag{44a}$$

$$\Lambda_{22} = \sum_{i,j} \frac{1}{4}\left[\tilde{T}^{(2)}_{PRi} T^{(2)}_{PRj} + 2\frac{k_B T}{\lambda} T^{(2)\prime}_{PRi} T^{(2)\prime}_{PRj}\right] \tag{44b}$$

where

$$\tilde{T}^{(2)}_{PR_i} = -\frac{\Delta G^0 + \lambda}{\lambda} \cdot 2 \sum_{I,J,K \in I} V_{PI} G^0_{IJ} \tilde{\lambda}_{Ji} G^0_{JK} V_{KR} \tag{45}$$

with $\tilde{\lambda}_{Ii}$ defined by eq (A4). Although Λ_{11} is independent of the bath index i, all the remaining terms include the components of reorganization energy, λ_i. In the present case, the sum of $2\tilde{\lambda}_{Ii}$

$$2\tilde{\lambda}_I = 2\sum_i \tilde{\lambda}_{Ii} = s_{\min I} - s_{\min R} \tag{46}$$

is the same order of magnitude of energy difference between the reactant and intermediate state at $s = s_{\min R}$. Thus the magnitude of factor $2\sum_J G^0_{IJ}\tilde{\lambda}_J G^0_{JK}$ appearing in Λ_{12} and Λ_{22} is comparable to G^0_{IK}. This explains the significant contributions from k_{12c} and k_{22c} as seen in Table 2.

Neglecting the second term of the right-hand side of eq 44b, which is considered to be small compared with the first term due to $2k_B T \ll \lambda$, the rate constant is written in the similar form of eq 2 as

$$k_c = \frac{1}{\hbar}|\bar{V}_{PR}|^2\left(\frac{\pi}{\lambda k_B T}\right)^{1/2} \exp\left[-\frac{\Delta G^{\ddagger}}{k_B T}\right] \quad (47)$$

where $\bar{V}_{PR}$ is the effective ECE given by

$$\bar{V}_{PR} = T^{(1)}_{PR} + \bar{T}^{(2)}_{PR} \quad (48a)$$

$$\bar{T}^{(2)}_{PR} = -\frac{\Delta G^0 + \lambda}{\lambda} \sum_{I,J,K\in I} V_{PI} G^0_{IJ} \tilde{\lambda}_J G^0_{JK} V_{KR} \quad (48b)$$

The effective ECE was estimated to be 5.06 cm^{-1}. Equation 47 provides the rate constant of 5.18×10^5 s^{-1}, which well reproduces the calculated value in Table 2, 5.16×10^5 s^{-1}.

$T^{(1)}_{PR}$ in the effective ECE is attributed to the electronic interaction between the zeroth-order electronic wave functions. It is noteworthy that $T^{(1)}_{PR}$ is similar to the electronic coupling in the gas phase, because $s_{\min R}$, the position on the solvation coordinate corresponding to $\mathbf{x} = \Delta_R$, is close to s_0^{solv} (see eq 34). The magnitude of $T^{(1)}_{PR}$ was calculated to be 4.02 cm^{-1}. In order to find out important electron propagation pathways, we carried out the decomposition analysis using the method previously developed.[10] $T^{(1)}_{PR}$ consists of the direct term $T^{(1)}_{PR\mathrm{dir}}$ and the indirect term $T^{(1)}_{PR\mathrm{indir}}$ as given by eq 9b

$$T^{(1)}_{PR} = T^{(1)}_{PR\mathrm{dir}} + T^{(1)}_{PR\mathrm{indir}} \quad (49a)$$

$$T^{(1)}_{PR\mathrm{dir}} = V_{PR} \quad (49b)$$

$$T^{(1)}_{PR\mathrm{indir}} = \sum_{I,J\in I} V_{PI} G^0_{IJ} V_{JR} \quad (49c)$$

$T^{(1)}_{PR\mathrm{dir}}$ represents the through space type interaction between R and P, and $T^{(1)}_{PR\mathrm{indir}}$ is of the through bond type indirect interaction. We further decomposed $T^{(1)}_{PR\mathrm{indir}}$ into several terms to distinguish the electron-transfer pathways. For this purpose, the intermediate states in eq 49c were classified into three subsets. The first consists of the states where the π^* orbitals of benzene part (π^*(Ben)) are occupied by the electron to be transferred. In the second subset, the single electron occupies the σ^* orbitals of the dimethyl groups attached to porphyrin (σ^*(DME)). The third one is constituted by the intermediate states where the remaining C−C and C−H σ^* orbitals are occupied (σ^*). $T^{(1)}_{PR\mathrm{indir}}$ was thus expressed as the sum of the contributions from the terms, $T^{(1)}_{PR\mathrm{indir}}$[A], $T^{(1)}_{PR\mathrm{indir}}$[A, B], and $T^{(1)}_{PR\mathrm{indir}}$[A, B, C], representing that the electron propagates through the intermediate subspace A, A and B, and A, B, and C, respectively. The explicit definitions and the methods of evaluation were presented in ref 10.

Table 3 summarizes the results of decomposition analysis. $T^{(1)}_{PR\mathrm{dir}}$ of 1.14 cm^{-1} was found to be less than half of $T^{(1)}_{PR\mathrm{indir}}$ of 2.88 cm^{-1}. The main contribution to $T^{(1)}_{PR\mathrm{indir}}$ is $T^{(1)}_{PR\mathrm{indir}}$[$\pi^*$(Ben)], 2.26 cm^{-1}, and the second important one is $T^{(1)}_{PR\mathrm{indir}}$[$\pi^*$(Ben), σ^*], 1.17 cm^{-1}. The π^* states of the benzene part are therefore considered to play an important role in determining $T^{(1)}_{PR\mathrm{indir}}$. It is noted that $T^{(1)}_{PR\mathrm{indir}}$[$\sigma^*$] is much smaller than $T^{(1)}_{PR\mathrm{indir}}$[$\pi^*$(Ben), σ^*], although both come from the electron pathways involving the states in the σ^* subset.

$\bar{T}^{(2)}_{PR}$ in the effective ECE, estimated to be 1.04 cm^{-1}, represents the Herzberg−Teller vibronic coupling, which is originated from the dependence of the transition matrix element on the bath coordinates. We performed the decomposition analysis to $\bar{T}^{(2)}_{PR}$ and the results are shown in Table 4. The dominant terms are found to be $\bar{T}^{(2)}_{PR}$[π^*(Ben)], 0.50 cm^{-1}, and $\bar{T}^{(2)}_{PR}$[π^*(Ben), σ^*], 0.48 cm^{-1}. It is noted that the relatively large contribution of $\bar{T}^{(2)}_{PR}$[π^*(Ben), σ^*] is due to the solvent effect of the intermediate states including σ^* orbitals, because the reorganization energies of these states, $\tilde{\lambda}_I$, are large in polar solvent, 40−60 kcal/mol.

TABLE 3: Transition Matrix Element $T^{(l)}_{PR}$ (cm^{-1})

	$T^{(l)}_{PR}$	$T^{(1)}_{PR\mathrm{indir}}[X]/T^{(1)}_{PR\mathrm{indir}}$
$T^{(l)}_{PR}$	4.02	
$T^{(l)}_{PR\mathrm{dir}}$	1.14	
$T^{(l)}_{PR\mathrm{indir}}$	2.88	
$T^{(l)}_{PR\mathrm{indir}}$[$\pi^*$(Ben)]	2.26	0.785
$T^{(l)}_{PR\mathrm{indir}}$[$\sigma^*$(DMe)]	−0.05	−0.017
$T^{(l)}_{PR\mathrm{indir}}$[$\sigma^*$]	−0.19	−0.066
$T^{(l)}_{PR\mathrm{indir}}$[$\pi^*$(Ben), σ^*(DMe)]	−0.09	−0.031
$T^{(l)}_{PR\mathrm{indir}}$[$\sigma^*$(DMe), σ^*]	−0.14	−0.049
$T^{(l)}_{PR\mathrm{indir}}$[$\pi^*$(Ben), σ^*]	1.17	0.406
$T^{(l)}_{PR\mathrm{indir}}$[$\pi^*$(Ben), σ^*(DMe), σ^*]	−0.08	−0.028

TABLE 4: Transition Matrix Element $\tilde{T}^{(l)}_{PR}$ (cm^{-1})

	$\tilde{T}^{(1)}_{PR}$	$\tilde{T}^{(l)}_{PR}[X]/\tilde{T}^{(1)}_{PR}$
$\tilde{T}^{(1)}_{PR}$	1.04	
$\tilde{T}^{(1)}_{PR}$[π^*(Ben)]	0.50	0.481
$\tilde{T}^{(1)}_{PR}$[σ^*(DMe)]	0.00	0.000
$\tilde{T}^{(1)}_{PR}$[σ^*]	0.14	0.135
$\tilde{T}^{(1)}_{PR}$[π^*(Ben), σ^*(DMe)]	−0.02	−0.019
$\tilde{T}^{(1)}_{PR}$[σ^*(DMe), σ^*]	−0.03	−0.029
$\tilde{T}^{(1)}_{PR}$[π^*(Ben), σ^*]	0.48	0.462
$\tilde{T}^{(1)}_{PR}$[π^*(Ben), σ^*(DMe), σ^*]	−0.03	−0.029

6. Concluding Remarks

In the present study, we investigated theoretically the reaction mechanism of long-range intramolecular electron-transfer process between the porphyrin and benzoquinone donor−acceptor pair mediated by an organic spacer in acetonitrile solvent. We focus on the effects of the solvent fluctuation on the reaction process.

The reaction rate expression including the dependence of the ECE on the solvent fluctuation was derived on the basis of Fermi's golden rule using the harmonic bath model. The rate constant was constituted by the standard TST constant and the terms involving the effects of solvent fluctuation.

We constructed a realistic molecular model by the ab initio MO calculations and performed the MD calculations to examine the effects of solvent fluctuation. The free energy curves of the reactant, product, and intermediate states along the solvation coordinate were determined. It was found that the free energy curves of the reactant and product are well-represented by harmonic ones and large solvation energy in the product state makes the reaction process exothermic, though the process is endothermic in the gas phase.

Using the quantities derived from the MO and MD calculations, the rate constant was estimated. It was demonstrated that the solvent effect on the ECE plays an important role in determining the rate constant. We further carried out the decomposition analyses for the ECEs. The characteristic electron pathways of the solvent-induced ECE were different from those of the ECE in the gas phase.

In the present study, we neglected the intramolecular conformational changes and vibrations. Although the effect of fluctuation of solute geometry may be important in determining the magnitude of the ECE element,[13,33,34] it is computationally too demanding to obtain the potential energies and electronic coupling elements as the functions of intramolecular coordinate. For the purpose, efficient methods would be required to construct the intramolecular functions. We will extend the present model to include the intramolecular dynamics in a future study.

Acknowledgment. Numerical calculations were carried out at Data Processing Center of Kyoto University and IMS Computer Center. This work was supported by the Grants in Aid for Scientific Research from the Ministry of Education. S. H. acknowledges the Research Fellowships of the Japan Society for the Promotion of Science for Young Scientists for support of this research.

Appendix A

The rate expressions of k_{12}, k_{13}, k_{14}, and k_{22} in eq 10 are presented. The classical expressions are not included here. These are easily derived from the semiclassical ones by replacing $k_B T_i' \rightarrow k_B T$.

(i) k_{12}:

$$k_{12sc} = \sum_i k_{12sci} \tag{A1}$$

$$k_{12sci} = \frac{1}{\hbar} T_{PR}^{(1)} T_{PRi}^{(2)\prime} \left(\frac{\pi}{\sum_j \lambda_j k_B T_j'} \right)^{1/2} L_{12sc}(\omega_i) \tag{A2}$$

where

$$T_{PRi}^{(2)\prime} = -2 \sum_{I,J,K \in I} V_{PI} G_{IJ}^0 \tilde{\lambda}_{Ji} G_{JK}^0 V_{KR} \tag{A3}$$

$$\tilde{\lambda}_{Ii} = \lambda_i \frac{g_I - g_R}{g_P - g_R} \tag{A4}$$

$$L_{12sc}(\omega_i) = E(0) - \left(\frac{1}{2} + \frac{k_B T_i'}{\hbar \omega_i} \right) E(\omega_i) - \left(\frac{1}{2} - \frac{k_B T_i'}{\hbar \omega_i} \right) E(-\omega_i) \tag{A5}$$

$$E(\omega) = \exp\left[- \frac{(\Delta G^0 + \hbar\omega + \lambda)^2}{4 \sum_i \lambda_i k_B T_i'} \right] \tag{A6}$$

(ii) k_{13}:

$$k_{13sc} = \sum_i k_{13sci} \tag{A7}$$

$$k_{13sci} = \frac{1}{\hbar} T_{PR}^{(1)} T_{PRi}^{(3)\prime} \left(\frac{\pi}{\sum_j \lambda_j k_B T_j'} \right)^{1/2} L_{13sc}(\omega_i) \tag{A8}$$

$$T_{PRi}^{(3)\prime} = 2 \sum_{I,J,K,L \in I} V_{PI} G_{IJ}^0 G_{JK}^0 \tilde{\lambda}_{Ki} G_{KL}^0 V_{LR} \hbar\omega_i \tag{A8}$$

$$L_{13sc}(\omega_i) = -2 \frac{k_B T_i'}{\hbar \omega_i} E(0) + \left(\frac{k_B T_i'}{\hbar \omega_i} + \frac{1}{2} \right) E(\omega_i) + \left(\frac{k_B T_i'}{\hbar \omega_i} - \frac{1}{2} \right) E(-\omega_i) \tag{A9}$$

(iii) k_{14}:

$$k_{14sc} = \sum_i k_{14sci} \tag{A10}$$

$$k_{14sci} = \frac{1}{\hbar} T_{PR}^{(1)} T_{PRi}^{(4)\prime} \left(\frac{\pi}{\sum_j \lambda_j k_B T_j'} \right)^{1/2} L_{14sc}(\omega_i) \tag{A11}$$

$$T_{PRi}^{(4)\prime} = T_{PR}^{(4)} \frac{\lambda_i}{\hbar^2} \tag{A12}$$

$$L_{14sc}(\omega_i) = \left\{ 6 \left(\frac{k_B T_i'}{\hbar \omega_i} \right)^2 - \frac{1}{2} \right\} E(0) - 2 \left\{ 2 \left(\frac{k_B T_i'}{\hbar \omega_i} \right)^2 + \frac{k_B T_i'}{\hbar \omega_i} \right\} E(\omega_i) - 2 \left\{ 2 \left(\frac{k_B T_i'}{\hbar \omega_i} \right)^2 - \frac{k_B T_i'}{\hbar \omega_i} \right\} E(-\omega_i) + \left(\frac{k_B T_i'}{\hbar \omega_i} + \frac{1}{2} \right)^2 E(2\omega_i) + \left(\frac{k_B T_i'}{\hbar \omega_i} - \frac{1}{2} \right)^2 E(-2\omega_i) \tag{A13}$$

(iv) k_{22}:

$$k_{22sc} = \sum_{i,j} k_{22scij} \tag{A14}$$

$$k_{22scij} = \frac{1}{\hbar} T_{PRi}^{(2)\prime} T_{PRj}^{(2)\prime} \left(\frac{\pi}{\sum_k \lambda_k k_B T_k'} \right)^{1/2} L_{22sc}(\omega_i, \omega_j) \tag{A15}$$

$$L_{22sc}(\omega_i, \omega_j) = \frac{1}{4} \left\{ E(0) - \left(\frac{1}{2} + \frac{k_B T_i'}{\hbar \omega_i} \right) E(\omega_i) - \left(\frac{1}{2} - \frac{k_B T_i'}{\hbar \omega_i} \right) E(-\omega_i) - \left(\frac{1}{2} + \frac{k_B T_j'}{\hbar \omega_j} \right) E(\omega_j) - \left(\frac{1}{2} - \frac{k_B T_j'}{\hbar \omega_j} \right) E(-\omega_j) + \left(\frac{1}{2} + \frac{k_B T_i'}{\hbar \omega_i} \right) \left(\frac{1}{2} + \frac{k_B T_j'}{\hbar \omega_j} \right) E(\omega_i + \omega_j) + \left(\frac{1}{2} - \frac{k_B T_i'}{\hbar \omega_i} \right) \left(\frac{1}{2} - \frac{k_B T_j'}{\hbar \omega_j} \right) E(-\omega_i - \omega_j) + \left(\frac{1}{2} + \frac{k_B T_i'}{\hbar \omega_i} \right) \left(\frac{1}{2} - \frac{k_B T_j'}{\hbar \omega_j} \right) E(\omega_i - \omega_j) + \left(\frac{1}{2} - \frac{k_B T_i'}{\hbar \omega_i} \right) \left(\frac{1}{2} + \frac{k_B T_j'}{\hbar \omega_j} \right) E(-\omega_i + \omega_j) \right\} \tag{A16}$$

Appendix B

Here we analyze the components of rate, k_{13c} and k_{13c}. The prefactor $\Lambda_{1\alpha}$ defined in eq 40 for those components are given by

$$\Lambda_{1\alpha} = \sum_i \sigma_{1\alpha}(\omega_i) T_{PR}^{(1)} T_{PRi}^{(2)\prime} \tag{B1}$$

with eqs A8 and A12. The dependences of the coefficients $\sigma_{1\alpha}$ in eq B1 on ω_i are illustrated in Figure 6, showing that σ_{13} is linear with respect to ω_i and σ_{14} is a quadratic function. Using the expansion of $E(\omega_i)$, eq 43, those coefficients are approximated by the lowest order terms

$$\sigma_{13}(\omega_i) = \left[h^{(1)} + 2 \frac{k_B T}{\hbar} h^{(2)} \right] \omega_i \tag{B2}$$

$$\sigma_{14}(\omega_i) = 2 h^{(2)} \omega_i^2 \tag{B3}$$

Note that the dependences on ω_i presented in Figure 6 are well-expressed by those approximated formulae. As a result, $\Lambda_{1\alpha}$ for $\alpha = 3, 4$ are represented by

$$\Lambda_{1\alpha} = \sum_i T^{(1)}_{PR} \tilde{T}^{(\alpha)}_{PRi} \tag{B4}$$

$$\tilde{T}^{(3)}_{PRi} = \left\{ -\frac{\Delta G^0 + \lambda}{2\lambda k_B T} - \frac{1}{2\lambda k_B T} + k_B T \left[\frac{\Delta G^0 + \lambda}{2\lambda k_B T} \right]^2 \right\} \times 2 \sum_{I,J,K,L \in I} V_{PI} G^0_{IJ} G^0_{JK} \tilde{\lambda}_{Ki} G^0_{KL} V_{KR} (\hbar\omega_i)^2 \tag{B5}$$

$$\tilde{T}^{(4)}_{PRi} = -\left\{ -\frac{1}{2\lambda k_B T} + \left[\frac{\Delta G^0 \lambda}{2\lambda k_B T} \right]^2 \right\} \times \frac{1}{2} \sum_{I,J,K \in I} V_{RI} G^0_{IJ} G^0_{JK} V_{KP} \lambda_i (\hbar\omega_i)^2 \tag{B6}$$

It is noteworthy that the magnitude of Λ_{13} is much smaller than that of Λ_{11} because the factor $\sum_J G^0_{IJ} \hbar\omega_i G^0_{JK}$ included in Λ_{13} is much smaller than G^0_{IK}. Λ_{14} is also much smaller than Λ_{13} because $\sigma_{14}(\omega_i)$ is very small in the main bath frequency region. These are consistent with the calculated results in Table 2.

References and Notes

(1) Wasielewski, M. R. *Chem. Rev.* **1992**, *92*, 435.
(2) Marcus, R. A.; Sutin, N. *Biochim. Biophys. Acta* **1985**, *811*, 265.
(3) Tang, J. *Chem. Phys. Lett.* **1994**, *217*, 55.
(4) Warshel, A.; Chu, Z. T.; Parson, W. W. *Science* **1989**, *246*, 112.
(5) Marchi, M.; Gehlen, J. N.; Chandler, D.; Newton, M. *J. Am. Chem. Soc.* **1993**, *115*, 4178.
(6) Treutlein, H.; Schulten, K.; Brunger, A. T.; Karplus, M.; Deisenhofer, J.; Michel, H. *Proc. Natl. Acad. Sci. U.S.A.* **1992**, *89*, 75.
(7) Schulten, K.; Tesch, M. *Chem. Phys.* **1991**, *158*, 421.
(8) Zheng, C.; McCammon, J. A.; Wolynes, P. G. *Chem. Phys.* **1991**, *158*, 261.
(9) Sakata, Y.; Nakashima, S.; Goto, Y.; Tatemitsu, H.; Misumi, S.; Asahi, T.; Hagihara, M.; Nishikawa, S.; Okada, T.; Mataga, N. *J. Am. Chem. Soc.* **1989**, *111*, 8979.
(10) Hayashi, S.; Kato, S. *J. Phys. Chem.*, in press.
(11) Kuznetsov, A. M.; Ulstrup, J. *J. Chem. Phys.* **1981**, *75*, 2047.
(12) Beratan, D. N.; Hopfield, J. J. *J. Chem. Phys.* **1984**, *81*, 5753.
(13) Freed, K. F.; Jortner, J. *J. Chem.. Phys.* **1970**, *52*, 6272.
(14) McConnell, H. M. *J. Chem. Phys.* **1961**, *35*, 508.
(15) We employed here the Basis 2 orbital set defined in ref 10.
(16) Kitagawa, S.; Morishima, I.; Yonezawa, T.; Sato, N. *Inorg. Chem.* **1979**, *18*, 1345.
(17) Lias, S. G.; Bartmess, J. E.; Holmes, J. H.; Levin, R. D.; Liebman, J. F.; Mallard, W. G. J. *Phys. Chem. Ref. Data* **1988**, *17*, 1.
(18) Eisner, U.; Linstead, P. P. *J. Chem. Soc. London* **1955**, 3749.
(19) Leggett, A. J.; Chakravarty, S.; Dorsey, A. T.; Fisher, M. P. A.; Garg, A.; Zwerger, W. *Rev. Mod. Phys.* **1987**, *59*, 1.
(20) Messiah, A. *Quantum Mechanics;* North-Holland: Amsterdam, 1965; Vol. 2.
(21) Siebrand, W. *Chem. Phys. Lett.* **1970**, *6*, 192.
(22) Henry, B. R.; Siebrand, W. *J. Chem. Phys.* **1971**, *54*, 1072.
(23) Hopfield, J. J. *Proc. Natl. Acad. Sci. U.S.A.* **1974**, *71*, 3640.
(24) Marcus, R. A. *J. Chem. Phys.* **1956**, *24*, 966.
(25) Marcus, R. A. *J. Chem. Phys.* **1956**, *24*, 979.
(26) H. Heitele *Angew. Chem., Int. Ed. Engl.* **1993**, *32*, 359.
(27) Hayashi, S.; Ando, K.; Kato, S. *J. Phys. Chem.* **1995**, *99*, 955.
(28) Ando, K.; Kato, S. *J. Chem. Phys.* **1991,** *95*, 5966.
(29) Jorgensen, W. L.; Briggs, J. M. *Mol. Phys.* **1988**, *63*, 547.
(30) Bayly, C.; Cieplak, P.; Cornell, W.; Kollman, P. A. *J. Phys. Chem.* **1993**, *97*, 10269.
(31) Cornell, W. D.; Cieplak, P.; Bayly, C. I.; Gould, I. R.; Merz, Jr., K. M.; Ferguson, D. M.; Spellmeyer, D. C.; Fox, T.; Caldwell, J. W.; Kollman, P. A. *J. Am. Chem. Soc.* **1995**, *117*, 5179.
(32) Arnold, K. E.; Yarwood, J.; Price, A. *H. Mol. Phys.* **1983**, *48*, 451.
(33) Efrima, S.; Bixon, M. *Chem. Phys. Lett.* **1974**, *25*, 34.
(34) Sumi, H. *J. Phys. Chem.* **1986**, *84*, 4272.